Model independent control of lightly damped noise/vibration systems

Jing Yuan[a)]
Department of Mechanical Engineering, The Hong Kong Polytechnic University, Hunghom, Kowloon, Hong Kong

(Received 21 March 2007; revised 28 April 2008; accepted 3 May 2008)

Feedforward control is a popular strategy of active noise/vibration control. In well-damped noise/vibration systems, path transfer functions from actuators to sensors can be modeled by finite impulse response (FIR) filters with negligible errors. It is possible to implement noninvasive model independent feedforward control by a recently proposed method called orthogonal adaptation. In lightly damped noise/vibration systems, however, path transfer functions have infinite impulse responses (IIRs) that cause difficulties in design and implementation of broadband feedforward controllers. A major source of difficulties is model error if IIR path transfer functions are approximated by FIR filters. In general, active control performance deteriorates as model error increases. In this study, a new method is proposed to design and implement model independent feedforward controllers for broadband in lightly damped noise/vibration systems. It is shown analytically that the proposed method is able to drive the convergence of a noninvasive model independent feedforward controller to improve broadband control in lightly damped noise/vibration systems. The controller is optimized in the minimum H_2 norm sense. Experiment results are presented to verify the analytical results. © *2008 Acoustical Society of America.*
[DOI: 10.1121/1.2936365]

PACS number(s): 43.50.Ki, 43.40.Vn, 43.40.Tm, 43.50.Gf [KA] Pages: 241–246

I. INTRODUCTION

Feedforward control is a popular strategy of active noise/vibration control[1,2] (ANVC) if the primary source is either available or recoverable as the reference signal. In many ANVC systems, path transfer functions from actuators to sensors are minimum required information. Parameters of a feedforward ANVC may be adaptive to generate destructive interference at sensed locations. The filtered-x least mean squares (FxLMS) algorithm is very popular for such a purpose. Stability of FxLMS depends on the accuracy of secondary path models. A FxLMS system may be unstable if phase errors in the secondary path model exceed 90°.[3–5] Since transfer functions in noise/vibration systems may change due to variation of boundary or environmental conditions, many ANVC systems adopt online modeling to keep path models as accurate as possible. These are called model independent feedforward controllers (MIFCs) for ease of reference.

Noise/vibration systems have different degrees of damping. In this study, a system is considered well damped if its path transfer functions can be modeled by finite impulse response (FIR) filters with negligible errors. Otherwise, the system is considered lightly damped. For well-damped noise/vibration systems, there are many MIFCs in the literature. Most of the available MIFCs require "persistent excitations"[6]—the invasive injection of probing signals[7] to ensure accurate online path modeling. Some researchers propose to avoid the probing signals by controller perturbation.[8–10] A noninvasive MIFC that abandons persistent excitations completely is possible by a method called orthogonal adaptation.[11]

For broadband control in lightly damped noise/vibration systems, it is difficult to implement noninvasive MIFC systems, since most noninvasive MIFC systems use FIR filters to approximate path transfer functions. Mismatches between FIR filters and infinite impulse response (IIR) path transfer functions degrade control performance. Although the performance difference between FIR and IIR models can be made arbitrarily small by increasing FIR filter taps, many researchers still propose ANVC systems with IIR path models or IIR controllers.[12–14] The main reason is to reduce coefficients, which means lower implementation costs, faster convergence rates, and better estimation accuracy. Adaptation of an IIR filter is a nonlinear process with multiple stationary points. There is no guarantee that an adaptive IIR filter will converge to its global optimal.[14] An adaptive ANVC, with FIR or IIR path models, has the same problem of either being model dependent or requiring invasive persistent excitations.

In this study, a modified MIFC system is proposed. It is a stable and noninvasive system for broadband control in lightly damped noise/vibration systems. It is also optimized in the minimum H_2 norm sense. These are significant differences between the modified MIFC and available ANVC systems with either FIR or IIR path models. Experimental results are presented to verify the modified MIFC when it is applied to lightly damped noise/vibration systems.

II. PROBLEM STATEMENT

In a noise/vibration system, the primary and secondary transfer functions are denoted by $P(z)$ and $S(z)$, respectively.

[a)]Electronic mail: mmjyuan@polyu.edu.hk

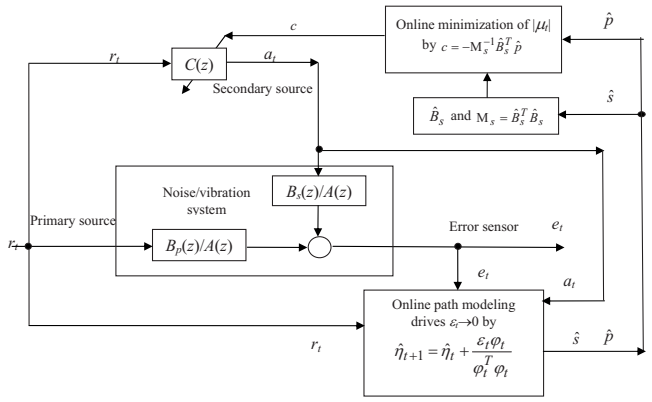

FIG. 1. Block diagram of the modified MIFC system.

If the primary source signal is either available or recoverable as the reference $r(z)$, the actuation signal $a(z)=C(z)r(z)$ may be synthesized by a controller whose transfer function is $C(z)$. The objective is destructive interference of the error signal modeled by

$$e(z)=P(z)r(z)+S(z)a(z)=[P(z)+S(z)C(z)]r(z). \quad (1)$$

In a lightly damped noise/vibration system, path models, $P(z)=B_p(z)/A(z)$ and $S(z)=B_s(z)/A(z)$ are IIR filters with a common denominator polynomial $A(z)$.[15] Equation (1) is equivalent to a discrete-time regression

$$e_t=-\sum_{k=1}^{m_r}\alpha_k e_{t-k}+\sum_{k=0}^{m}p_k r_{t-k}+\sum_{k=0}^{m}s_k a_{t-k}, \quad (2)$$

where $\{\alpha_k\}$, $\{p_k\}$, and $\{s_k\}$ are coefficients of polynomials $A(z)$, $B_p(z)$, and $B_s(z)$. Introducing coefficient vector $\eta^T=[-\alpha^T,p^T,s^T]$ and regression vector $\varphi_t=[e_{t-1},e_{t-2},\ldots,e_{t-m_r},r_t,r_{t-1},\ldots,r_{t-m},a_t,a_{t-1},\ldots,a_{t-m}]^T$, one may express Eq. (2) as

$$e_t=\eta^T\varphi_t=-\alpha^T x_t+p^T\upsilon_t+s^T\phi_t, \quad (3)$$

where $x_t=[e_{t-1},e_{t-2},\ldots,e_{t-m_r}]^T$, $\upsilon_t=[r_t,r_{t-1},\ldots,r_{t-m}]^T$, and $\phi_t=[a_t,a_{t-1},\ldots,a_{t-m}]^T$. Since the regression vector φ_t and its subvector ϕ_t contain actuation signal a_t, different controllers are designed to regulate ϕ_t and minimize $|e_t|=|\eta^T\varphi_t|$.

In this study, a noninvasive MIFC is proposed for broadband control in lightly damped noise/vibration systems. It is described by the block diagram in Fig. 1. A recursive least squares (RLS) algorithm is applied for online path modeling. Estimates of $A(z)$, $B_p(z)$, and $B_s(z)$ are denoted by $\hat{A}(z)$, $\hat{B}_p(z)$, and $\hat{B}_s(z)$, respectively. The estimated parameter vector is denoted by $\hat{\eta}^T=[\hat{\alpha}^T,\hat{p}^T,\hat{s}]$, where $\hat{\alpha}$, $\hat{p}$, and $\hat{s}$ consist of coefficients of $\hat{A}(z)$, $\hat{B}_p(z)$, and $\hat{B}_s(z)$, respectively. Estimation residue is calculated as

$$\varepsilon_t=e_t-\hat{\eta}^T\varphi_t=\Delta\eta^T\varphi_t=-\Delta\alpha^T x_t+\Delta p^T\upsilon_t+\Delta s^T\phi_t, \quad (4)$$

where $\Delta\eta=\eta-\hat{\eta}$, $\Delta\alpha=\alpha-\hat{\alpha}$, $\Delta p=p-\hat{p}$, and $\Delta s=s-\hat{s}$. The objective of online modeling is to drive $\varepsilon_t\to 0$. This task is represented by a block below the noise/vibration system in Fig. 1, with inputs r_t, a_t, and e_t for construction of φ_t.

Part of the online estimates, $\hat{p}$ and $\hat{s}$, are used in Fig. 1 to solve optimal controller $C(z)$ and minimize $\|\hat{B}_p(z)+\hat{B}_s(z)C(z)\|_2$. In broadband noise control, power spectral density of $r(z)$ is nearly constant in the entire frequency range. Minimizing $\|\hat{B}_p(z)+\hat{B}_s(z)C(z)\|_2$ is equivalent to minimizing magnitude of

$$\mu_t=\sum_{k=0}^{m}\hat{p}_k r_{t-k}+\sum_{k=0}^{m}\hat{s}_k a_{t-k}=\hat{p}^T\upsilon_t+\hat{s}^T\phi_t. \quad (5)$$

One may study the joint effects of the two online tasks by using $\mu_t=\hat{p}^T\upsilon_t+\hat{s}^T\phi_t$, Eqs. (3) and (4) to derive

$$|e_t+\hat{\alpha}^T x_t|=|\varepsilon_t+\mu_t|\leqslant|\varepsilon_t|+|\mu_t|. \quad (6)$$

In the rest of this paper, it will be shown that (i) the RLS algorithm will drive the convergence of $\varepsilon_t\to 0$, and the online optimization task will force $\mu_t\approx 0$; (ii) $e_t+\hat{\alpha}^T x_t\approx 0$ is implied by (i) and is equivalent to $\hat{A}(z)e(z)\approx 0$; (iii) in broadband control, $\varepsilon_t\to 0$ implies $\hat{A}(z)\to A(z)$ and therefore $\hat{A}(z)e(z)\approx 0$ will be equivalent to $A(z)e_t\approx 0$; (iv) the modified MIFC is noninvasive and optimal and it minimizes $\|\hat{B}_p(z)+\hat{B}_s(z)C(z)\|_2$ without persistent excitations.

III. ONLINE MODELING

A simple RLS algorithm is applied to drive $\varepsilon_t=\Delta\eta^T\varphi_t\to 0$ in this section. The estimated parameter vector is updated by

$$\hat{\eta}_{t+1}=\hat{\eta}_t+\frac{\varepsilon_t\varphi_t}{\varphi_t^T\varphi_t}. \quad (7)$$

A positive definite function $V(t)=\Delta\eta_t^T\Delta\eta_t$ is introduced here to analyze the convergence of Eq. (7). Similar to identity $a^2-b^2=(a-b)(a+b)$, it can be shown that

$$V(t+1)-V(t)=(\Delta\eta_{t+1}-\Delta\eta_t)^T(\Delta\eta_{t+1}+\Delta\eta_t). \quad (8)$$

With the help of Eq. (7) and $\Delta\eta=\eta-\hat{\eta}$, one can see that

$$\Delta\eta_{t+1}-\Delta\eta_t=\hat{\eta}_t-\hat{\eta}_{t+1}=\frac{-\varepsilon_t\varphi_t}{\varphi_t^T\varphi_t} \quad (9)$$

and

$$\Delta\eta_{t+1}+\Delta\eta_t=2\eta-\hat{\eta}_t-\hat{\eta}_{t+1}=2\Delta\eta_t-\frac{\varepsilon_t\varphi_t}{\varphi_t^T\varphi_t}. \quad (10)$$

By substituting Eqs. (9) and (10) into Eq. (8), one can derive

$$V(t+1)-V(\mathrm{t})=\frac{-\varepsilon_t\varphi_t^T}{\varphi_t^T\varphi_t}\left(2\Delta\eta_t-\frac{\varepsilon_t\varphi_t}{\varphi_t^T\varphi_t}\right). \quad (11)$$

Since $\varepsilon_t\varphi_t^T\Delta\eta_t=\varepsilon_t^2$, the above equation is equivalent to

$$V(t+1)-V(t)=-\frac{\varepsilon_t^2}{\phi^T\phi}\leqslant 0. \quad (12)$$

This indicates monotonous decrease of $V(t)=\Delta\eta_t^T\Delta\eta_t$ until $\varepsilon_t\to 0$.

IV. ONLINE OPTIMIZATION

If $\hat{B}_s(z)$ is minimum phase, an IIR filter $C(z)=-\hat{B}_s^{-1}(z)\hat{B}_p(z)$ will achieve $\mu_t=0$. In case $\hat{B}_s(z)$ is nonmini-

mum phase, $\hat{B}_s^{-1}(z)$ is unstable and a different $C(z)$ must be sought. Although it takes an IIR $C(z)$ to minimize $\|\hat{B}_p(z)+\hat{B}_s(z)C(z)\|_2$ to the best extent,[11] a FIR $C(z)$ is sought here to minimize

$$\|\hat{B}_p(z)+\hat{B}_s(z)C(z)\|_2=\|\hat{B}(z)\|_2 \tag{13}$$

while reducing online computations.

Let n denote the degree of $C(z)$. The impulse response of Eq. (13) is given by

$$\hat{b}=\begin{bmatrix}\hat{b}_0\\ \hat{b}_1\\ \vdots\\ \\ \vdots\\ \hat{b}_{m+n}\end{bmatrix}=\begin{bmatrix}\hat{p}_0\\ \hat{p}_1\\ \vdots\\ \hat{p}_m\end{bmatrix}+\begin{bmatrix}\hat{s}_0 & & & \\ \hat{s}_1 & \hat{s}_0 & & \\ \vdots & \hat{s}_1 & \ddots & \\ \hat{s}_m & \vdots & \ddots & \hat{s}_0\\ & \hat{s}_m & \vdots & \hat{s}_1\\ & & \ddots & \vdots\\ & & & \hat{s}_m\end{bmatrix}\begin{bmatrix}c_0\\ c_1\\ \vdots\\ c_n\end{bmatrix}$$

$$=\hat{b}_p+\hat{B}_s c, \tag{14}$$

where $\hat{b}=[\hat{b}_0,\ldots,\hat{b}_{m+n}]^T$ and $c=[c_0,\ldots,c_n]^T$ are coefficient vectors of $\hat{B}(z)$ and $C(z)$. Coefficients of $\hat{B}_s(z)$ are used to construct an n-column matrix

$$\hat{B}_s=\begin{bmatrix}\hat{s}_0 & & & \\ \hat{s}_1 & \hat{s}_0 & & \\ \vdots & \hat{s}_1 & \ddots & \\ \hat{s}_m & \vdots & \ddots & \hat{s}_0\\ & \hat{s}_m & \vdots & \hat{s}_1\\ & & \ddots & \vdots\\ & & & \hat{s}_m\end{bmatrix}. \tag{15}$$

The rank of $\hat{B}_s$ is n if $\hat{B}_s(z)\neq 0$, since $\hat{B}_s$ contains an $n\times n$ triangular submatrix.

According to Parserval's theorem, minimizing $\|\hat{b}\|^2$ is equivalent to minimizing Eq. (13). Equation (14) is equivalent to

$$\hat{b}^T\hat{b}=(\hat{p}+\hat{B}_s c)^T(\hat{p}+\hat{B}_s c)$$

$$=\hat{p}^T\hat{p}+\hat{p}^T\hat{B}_s c+c^T\hat{B}_s^T\hat{p}+c^T M_s c, \tag{16}$$

where $M_s=\hat{B}_s^T\hat{B}_s$ is the autocorrelation matrix of $\hat{B}_s(z)$. Let $\zeta=\hat{B}_s^T\hat{p}$, then one can use $c^T\hat{B}_s^T\hat{p}=c^T M_s M_s^{-1}\zeta$ to rewrite Eq. (16) as

$$\hat{b}^T\hat{b}=\hat{p}^T\hat{p}-\zeta^T M_s^{-1}\zeta+(M_s c+\zeta)^T M_s^{-1}(M_s c+\zeta). \tag{17}$$

In Eq. (17), vector c only affects $(M_s c+\zeta)^T M_s^{-1}(M_s c+\zeta)$. Therefore it is possible to force $(M_s c+\zeta)^T M_s^{-1}(M_s c+\zeta)=0$ and minimize $\|\hat{b}\|^2$ by

$$c=-M_s^{-1}\zeta=-M_s^{-1}\hat{B}_s^T\hat{p}. \tag{18}$$

This equation is used to obtain parameters of suboptimal FIR filter $C(z)$ in Fig. 1.

V. PARAMETER CONVERGENCE

With online tasks driving $\varepsilon_t\to 0$ and $\mu_t\approx 0$, one can see $e_t+\hat{\alpha}^T x_t\approx 0$ in Eq. (6). Since $\hat{A}(z)=1+\sum_{k=1}^{m_r}\hat{\alpha}_k z^{-k}$ and $x_t=[e_{t-1},e_{t-2},\ldots,e_{t-m_r}]^T$, it follows that $e_t+\hat{\alpha}^T x_t\approx 0$ is equivalent to $\hat{A}(z)e(z)\approx 0$. However, this does not indicate the minimization of $|e_t|$ until it is proven that $\hat{A}(z)\to A(z)$.

Let $B(z)=B_p(z)+B_s(z)C(z)$, then one can obtain an equivalent expression of Eq. (3) as

$$e_t=-\sum_{k=1}^{m_r}\alpha_k e_{t-k}+\sum_{k=0}^{2m}b_k r_{t-k}, \tag{19}$$

where $\{b_k\}$ are coefficients of $B(z)=B_p(z)+B_s(z)C(z)$. Estimate of $B(z)$ is denoted by $\hat{B}(z)$ and defined in Eq. (13). Similar to the derivation of Eq. (4), one can obtain

$$\varepsilon_t=-\sum_{k=1}^{m_r}\Delta\alpha_k e_{t-k}+\sum_{k=0}^{2m}\Delta b_k r_{t-k}, \tag{20}$$

where $\{\Delta\alpha_k=\alpha_k-\hat{\alpha}_k\}$ and $\{\Delta b_k=b_k-\hat{b}_k\}$ are estimation errors of $A(z)$ and $B(z)$, respectively. In Ref. 6, it is shown that convergence of $\varepsilon_t=\varphi_t^T\Delta\eta\to 0$ implies

$$\begin{bmatrix} e_{t-l} & e_{t-l-1} & \cdots & e_{t-m_r-l+1} & r_{t-l-1} & r_{t-l-2} & \cdots & r_{t-m-n-l}\\ e_{t-l+1} & e_{t-l} & \cdots & e_{t-m_r-l+2} & r_{t-l} & r_{t-l-1} & \cdots & r_{t-m-n-l+1}\\ \vdots & \vdots & \cdots & \vdots & \vdots & \vdots & \cdots & \vdots\\ e_{t-2} & e_{t-3} & \cdots & e_{t-m_r-1} & r_{t-1} & r_{t-2} & \cdots & r_{t-m-n-1}\\ e_{t-1} & e_{t-2} & \cdots & e_{t-m_r} & r_t & r_{t-1} & \cdots & r_{t-m-n}\end{bmatrix}\begin{bmatrix}\Delta\alpha_1\\ \Delta\alpha_2\\ \vdots\\ \Delta\alpha_{m_r}\\ -\Delta b_0\\ -\Delta b_1\\ \vdots\\ -\Delta b_{m+n}\end{bmatrix}\to 0. \tag{21}$$

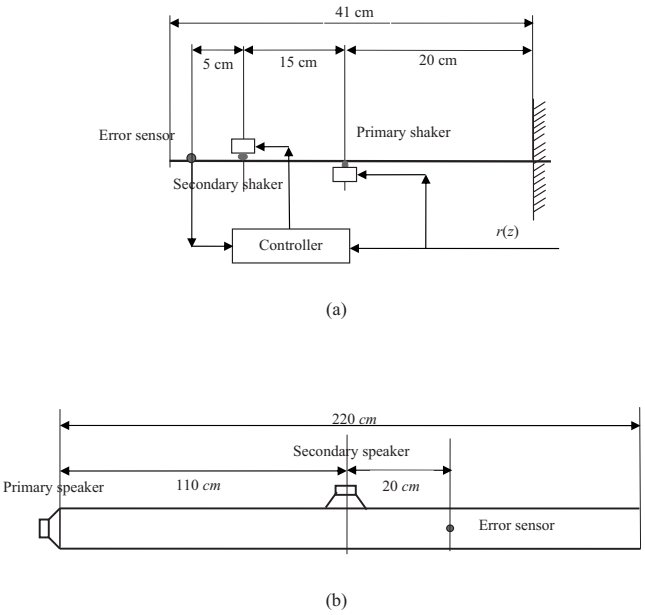

FIG. 2. Experiment setup: (a) top view of vibration system and (b) noise system.

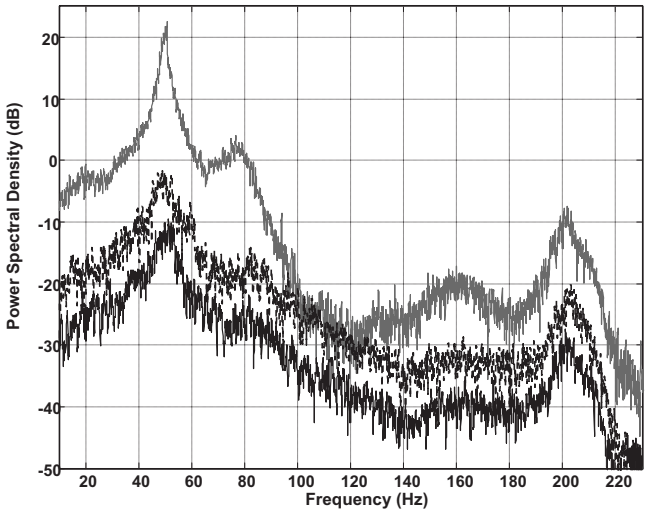

FIG. 3. Normalized PSD of error signal in experiment 1: uncontrolled (gray), controlled by an ordinary MIFC (dashed black), and controlled by the modified MIFC (solid black).

Here $t>l\geqslant m_r+m+n+1$. If r_t contains more than $0.5(m_r+m+n+1)$ frequency components, then the above data matrix is full rank[6] and $\varepsilon_t\rightarrow 0$ implies $\{\Delta\alpha_k\rightarrow 0\}$ and $\{\Delta b_k\rightarrow 0\}$. As a result, $\hat{A}(z)e(z)\approx 0$ converges to $A(z)e(z)\approx 0$ in broadband control operations and stability of $|e_t|$ is ensured by the modified MIFC.

The z-transform domain version of Eq. (19) is $A(z)e(z)=B(z)r(z)$, where $A(z)$ and $B(z)$ are, respectively, the autoregressive and moving-average parts. A feedforward controller can only minimize the moving-average part $\|B(z)\|_2$. After the convergence of $\hat{B}(z)\rightarrow B(z)$, there are infinitely many pairs of $\hat{B}_p(z)$ and $\hat{B}_s(z)$ satisfying $\hat{B}_p(z)+\hat{B}_s(z)C(z)=B(z)$, from which only one pair matches $B_p(z)$ and $B_s(z)$ exactly. When an accurate $\hat{B}_s(z)$ is required to ensure stable adaptation of FxLMS, the only available way to drive $\hat{B}_s(z)\rightarrow B_s(z)$ is persistent excitation in the actuation signal.

A significant feature of the modified MIFC is online optimization instead of FxLMS. Analytically, one may write

$$\|B(z)\|_2=\|\Delta B(z)+\hat{B}_p(z)+\hat{B}_s(z)C(z)\|_2 \leqslant \|\Delta B(z)\|_2+\|\hat{B}_p(z)+\hat{B}_s(z)C(z)\|_2. \quad (22)$$

Since $\varepsilon_t\rightarrow 0$ implies $\|\Delta B(z)\|_2\rightarrow 0$ and $\mu_t\approx 0$ is the result of minimizing $\|\hat{B}_p(z)+\hat{B}_s(z)C(z)\|_2$, the modified MIFC minimizes $\|B(z)\|_2$ by the joint effects of online tasks. The objective is achieved without persistent excitation.

VI. EXPERIMENTS

In this study, three experiments were conducted to demonstrate advantages of the modified MIFC. The experiment setups are shown in Figs. 2(a) and 2(b), respectively. In the experiments, the controllers were implemented in a dSPACE 1103 board, and the primary source $r(z)$ was a broadband pseudorandom signal. While it is possible to recover $r(z)$ from a measured signal, it would require additional online modeling of feedback path and cancelation of actuation feedback. To simplify programming, $r(z)$ was directly available to the controller in all experiments.

A. A well-damped vibration system

The first experiment was conducted to test an ordinary MIFC in a well-damped vibration system. Major dimensional information is given in Fig. 2(a). Cross-sectional area of the steel beam was 50×1.5 mm^2. The error sensor was a B&K 4382 accelerometer. The system sampling rate was 500 Hz. All signals were low-pass filtered with cutoff frequency of 200 Hz. Both actuators were shakers with shafts connected to the beam and solenoids attached to fixed bases. Damping coefficients of the shakers were different since the shakers were made by different manufacturers. The primary shaker was one with weak damping and the secondary shaker was one with strong damping.

The controllers were turned off first to collect the error signal $e(z)$. Power spectral densities (PSDs) of $e(z)$ and $r(z)$ were computed with the MATLAB command "pmtm( )" and denoted as P_e=pmtm(e) and P_r=pmtm(r), respectively. Here e and r are vectors containing data of $e(z)$ and $r(z)$. The normalize PSD of $e(z)$ is calculated as $P_{ne}=10\log(P_e/P_r)$ and plotted as the gray curve in Fig. 3. It is the reference for comparison. The PSD indicates a well-damped vibration system with fat resonant peaks.

An ordinary MIFC, proposed in Ref. 11, was tested first. The degrees of $C(z)$, $\hat{P}(z)$, and $\hat{S}(z)$ were $n=m=300$. The total number of adaptive coefficients was 900. The dashed-black curve in Fig. 3 represents the normalized PSD of the error signal collected after the convergence of the ordinary MIFC. Since the system was well damped, the ordinary MIFC was able to suppress vibration with reasonably good control performance.

The modified MIFC system was then tested under the same experimental conditions. The degrees of $\hat{A}(z)$, $C(z)$, and $\hat{B}_p(z)$ and $\hat{B}_s(z)$ were $m_r=100$, $n=300$, and $m=200$. The

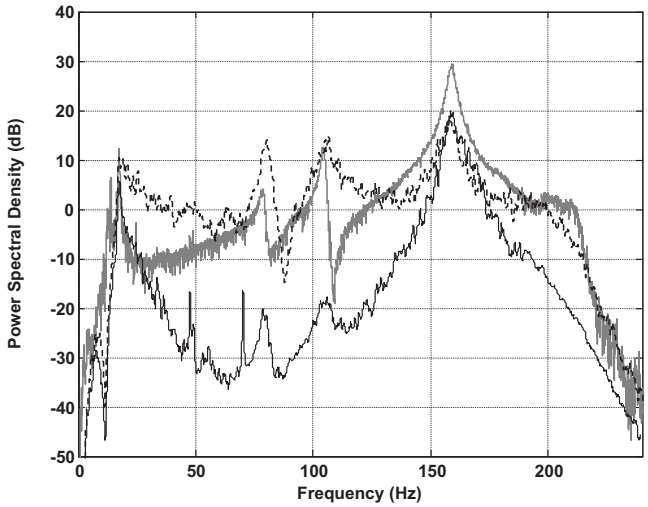

FIG. 4. Normalized PSD of error signal in experiment 2: uncontrolled (gray), controlled by an ordinary MIFC (dashed black), and controlled by the modified MIFC (solid black).

total number of adaptive coefficients was 800, which was almost the same as the ordinary MIFC system. Normalized PSD of the error signal was obtained after the convergence of the modified MIFC system. It is plotted as the solid-black curve in Fig. 3. The modified MIFC system improved control performance in the entire frequency range of interests. The improvement was not very significant since this was a well-damped system with negligible errors between transfer functions and FIR path models.

B. A lightly damped vibration system

In the second experiment, the setup was almost the same as in the first case. Only the secondary shaker was replaced by an inertial actuator with very weak damping. The inertial actuator was attached to the beam without other support. Its mass caused significant loading effect and reduced the fundamental frequency of the vibration system. The system sampling rate was still 500 samples/s and all signals were low-pass filtered with cutoff frequency of 200 Hz.

Again, the controllers were turned off first to collect the error signal $e(z)$. The normalized PSD of $e(z)$ is shown as the gray curve in Fig. 4. With very weak damping in both primary and secondary actuators, the system became lightly damped. In particular, the low-frequency resonant peaks of the PSD are very narrow, which implies IIR path transfer functions.

The ordinary MIFC was implemented and tested. The degrees of $C(z)$, $\hat{P}(z)$, and $\hat{S}(z)$ were $n=m=300$. The dashed-black curve in Fig. 4 represents the normalized PSD of the error signal collected after the convergence of the ordinary MIFC. Although the ordinary MIFC suppressed vibration, the effect was not significant. The controller even enhanced vibration in some frequencies. An important reason for the poor performance is the model error in approximating IIR path transfer functions with FIR filters.

The modified MIFC was then implemented and the degrees of $\hat{A}(z)$, $C(z)$, and $\hat{B}_p(z)$ and $\hat{B}_s(z)$ were $m_r=100$, $n=300$, and $m=200$. The solid-black curve in Fig. 4 represents the normalized PSD of the error signal collected after the convergence of the modified MIFC. Comparing all curves in Fig. 4, one can see that the modified MIFC suppressed vibration much more significantly. The complexity of the ordinary MIFC was 300 coefficients for $P(z)$, $S(z)$, and $C(z)$, respectively, with a total number of 900 coefficients. The complexity of the modified MIFC was 100 coefficients for $A(z)$, 200 coefficients for $B_p(z)$, $B_s(z)$, and 300 coefficients for $C(z)$, with a total number of 800 coefficients. The modified MIFC system improved control performance significantly with almost the same complexity in terms of adaptive coefficients.

In experiment 2, the beam was so lightly damped that its vibration, if caused by an impulsive impact, would last for at least 6 s. The long-lasting impulse response must be modeled by a FIR filter with at least $m=3000$ taps when the sampling rate was 500 Hz. The author did not have the fast hardware to test a MIFC with so many adaptive coefficients. Increasing FIR filter taps has other negative effects because convergence rate and estimation accuracy of system identification algorithms are related to rank and condition number of the data matrix in Eq. (21).[6] Here the matrix had $l=m_r+m+n+1=601$ columns for the modified MIFC, but at least $l=m+n+1=3301$ columns for the ordinary MIFC if the FIR path model had been increased to $m=3000$ taps while $n=300$ unchanged. More than five times of columns in the data matrix of Eq. (21) would have required more than five times longer t to meet the necessary full rank condition. It means a much slower convergence rate. Besides, condition number of a large matrix is sensitive to quantization errors, finite word-length effects, etc. With a large size, the data matrix of Eq. (21) may have been analytically full rank, but numerically ill conditioned to degrade estimate accuracy. The modified MIFC is preferred with lower implementation cost, faster convergence rate, and better estimation accuracy due to a much smaller data matrix in Eq. (21).

C. A noise control system

The third experiment was conducted to test the modified MIFC for noise control. Major dimensional information is given in Fig. 2(b). Cross-sectional area of the duct was 11×14.5 cm^2. The system sampling rate was 2.7 kHz samples/s and all signals were low-pass filtered with cutoff frequency of 1.2 kHz. Similar to the previous two experiments, the controllers were turned off first to collect the error signal $e(z)$. The normalized PSD of $e(z)$ is represented by the gray curve in Fig. 5. The experimental duct is not very lightly damped since resonant peaks of the PSD are not as narrow as those in Fig. 4.

The ordinary MIFC was tested. The degrees of $C(z)$, $\hat{P}(z)$, and $\hat{S}(z)$ were $n=m=300$. The dashed-black curve in Fig. 5 represents the normalized PSD of the error signal obtained after the convergence of the ordinary MIFC. The ordinary MIFC suppressed noise better than it did in vibration control. In all experiments, the ordinary MIFC had the same complexity but the control performances were different. An important reason is model error in approximating IIR path transfer functions with FIR models.

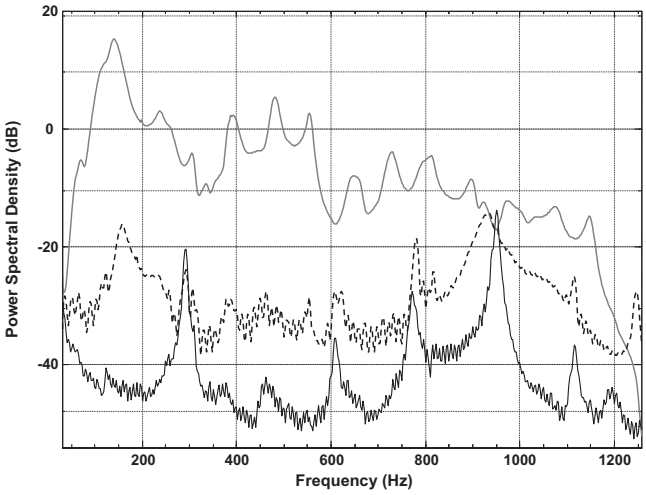

FIG. 5. Normalized PSD of error signal in experiment 3: uncontrolled (gray), controlled by an ordinary MIFC (dashed black), and controlled by the modified MIFC (solid black).

The modified MIFC was also tested in case 3. The degrees of $\hat{A}(z)$, $C(z)$, and $\hat{B}_p(z)$ and $\hat{B}_s(z)$ were $m_r=100$, $n=300$, and $m=200$. The solid-black curve in Fig. 5 represents the normalized PSD of the error signal collected after the convergence of the modified MIFC. Comparing all curves in Fig. 5, one can see that the modified MIFC improved noise control significantly in the entire frequency range of interest. Similar to case 2, the complexity of the ordinary MIFC was 300 coefficients for $P(z)$, $S(z)$, and $C(z)$, respectively, with a total number of 900 coefficients. The complexity of the modified MIFC was 100 coefficients for $A(z)$, 200 coefficients for $B_p(z)$ and $B_s(z)$, and 300 coefficients for $C(z)$, with a total number of 800 coefficients. Again, the modified MIFC system improved performance significantly with almost the same complexity in terms of adaptive coefficients.

Similar to experiment 2, the ordinary MIFC system may improve its performance by increasing FIR filter taps. That means higher implementation cost, slower convergence rate, and potentially worse estimation accuracy.

VII. CONCLUSION

It is more difficult to design and implement MIFC for lightly damped noise/vibration systems. The difficulty becomes worse as the degree of damping reduces. A modified MIFC is proposed here to improve broadband control in such systems, with modified online modeling to identify IIR path models. The controller is optimized by an online algorithm that only uses the numerators of IIR path estimates. It is shown analytically that the modified MIFC is noninvasive, stable, and able to improve broadband control in lightly damped noise/vibration systems. Experimental results are presented to verify the analytical results.

[1]C. H. Hansen and S. D. Snyder, *Active Control of Noise and Vibration* (E and FN Spon, London, 1997).
[2]P. A. Nelson and S. J. Elliott, *Active Control of Sound* (Academic, London, 1992).
[3]M. A. Vaudrey, W. T. Baumann, and W. R. Saunders, "Stability and operation constraints of adaptive LMS-based feedback control," Automatica **39**, 595–605 (2003).
[4]E. Bjarnason, "Analysis of the filtered-x LMS algorithm," IEEE Trans. Speech Audio Process. **3**, 504–514 (1995).
[5]S. D. Snyder and C. H. Hansen, "The influence of transducer transfer functions and acoustic time delay on the LMS algorithm in active noise control systems," J. Sound Vib. **140**, 409–424 (1990).
[6]G. C. Goodwin and K. S. Sin, *Adaptive Filtering, Prediction and Control* (Prentice-Hall, Englwood Cliffs, NJ, 1984).
[7]L. J. Eriksson and M. C. Allie, "Use of random noise for on-line transducer modeling in an adaptive active attenuation system," J. Acoust. Soc. Am. **85**, 797–802 (1989).
[8]W. C. Nowlin, G. S. Guthart, and G. K. Toth, "Noninvasive system identification for multichannel broadband active noise control," J. Acoust. Soc. Am. **107**, 2049–2060 (2000).
[9]X. Qiu and C. H. Hansen, "An algorithm for active control of transformer noise with on-line cancellation path modelling based on the perturbation method," J. Sound Vib. **240**, 647–665 (2001).
[10]B. J. Kim and D. C. Swanson, "Linear independence method for system identification/secondary path modeling for active control," J. Acoust. Soc. Am. **118**, 1452–1468 (2005).
[11]J. Yuan, "Orthogonal adaptation for active noise control," J. Acoust. Soc. Am. **120**, 204–210 (2006).
[12]L. J. Eriksson, "Development of the filtered-u algorithm for active noise control," J. Acoust. Soc. Am. **89**, 257–265 (1991).
[13]J. Lu, C. Shen, X. Qiu, and B. Xu, "Lattice form adaptive infinite impulse response filtering algorithm for active noise control," J. Acoust. Soc. Am. **113**, 327–335 (2003).
[14]P. A. Regalia, *Adaptive IIR Filtering in Signal Processing and Control* (Dekker, New York, 1995).
[15]J. S. Vipperman and R. A. Burdisso, "Adaptive feedforward control of non-minimum phase structural systems," J. Sound Vib. **183**, 369–382 (1995).